Experimental and numerical investigations on determination of strain localization in sheet forming

IOP Conf. Series: Journal of Physics: Conf. Series **1063** (2018) 012060 doi:10.1088/1742-6596/1063/1/012060

Experimental and numerical investigations on determination of strain localization in sheet forming

D. Lumelskyj[1], L. Lazarescu[2], D. Banabic[2], J. Rojek[1]

[1]Institute of Fundamental Technological Research, Polish Academy of Sciences, Pawińskiego 5B, 02-106 Warsaw, Poland
[2]Center of Research for Sheet Metal Forming Technology "CERTETA", Technical University of Cluj-Napoca, Memorandumului 28, 400114, Cluj Napoca, Romania

E-mail: dlumelsk@ippt.pan.pl

Abstract.

This work presents results of investigations on the determination of strain localization in sheet forming. Nakajima formability test has been chosen for the experimental studies and numerical analysis. The onset of localized necking has been determined using the criteria studied in the authors' earlier works, based on the analysis of the principal strains evolution in time. The first criterion is based on the analysis of the through-thickness thinning (through–thickness strain) and its first time derivative in the most strained zone. The limit strain in the second method is determined by the maximum of the strain acceleration. Limit strains obtained from these criteria have been confronted with the experimental forming limit curve (FLC) evaluated according to modified Bragard method used in the ISO standard. The comparison shows that the first criterion predicts formability limits closer to the experimental FLC and second method predicts values of strains higher than FLC. These values are closer to the maximum strains measured before fracture appears in experiment. These investigations show that criteria based on the analysis of strain evolution used in numerical simulation and experimental studies allow us to determine strain localization.

1. Introduction

Analysis of formability in sheet forming operations is still a subject of research works [1, 2, 3]. In the engineering practice the strain based forming limit diagrams (FLD) are the most commonly used tools to validate sheet metal formability. The forming limit curve (FLC) on the FLD is the principal strain locus determined by the failure in the form of strain localization or material fracture. There are many approaches to evaluate the FLCs including experimental [4], theoretical [5], as well as hybrid methods combining experimental data with analytical or numerical approaches [6]. An overview of methods of FLC determination is presented in [7].

Theoretical methods are based on criteria of the loss of stability (strain localization) or damage (fracture) of the material. Over the past few decades, theoretical methods received significant progress. Despite that, the most reliable approaches for evaluation of formability are based on the experimental methods. Nakajima [4] test considered in this work is one of the most often used experimental methods. The strains during the experiments are measured automatically using systems such as AutoGrid, ASAME or ARAMIS. The limit strains (forming limits) can be calculated using different methods [7] proposed by Veerman , Bragard, Kobayashi,

Hecker and others based on the analysis of the strains measured in the critical zone. The modified Bragard method is used in the standard ISO 12004-2 [4].

Along with the evolution of measurement systems, new methods for determining limit strains have been developed. There is a group of the algorithms based on the analysis of time evolution (t-d method) of strains and their time derivatives. Volk and Hora [8] have presented a method based on the analysis of the first derivative of the strains in the necked zone. The onset of necking is assumed to occur at the point corresponding to a sudden change of the slope of the strain rate vs. time curve. The first and second time derivatives of the principal strains (strain velocities and accelerations) have been postprocessed in [5]. The onset of necking is determined by the peak of the major strain acceleration vs. time curve. Martnez-Donaire et. al [9] propose the t-d method in which the onset of necking was detected by the appearance of a maximum in the first time derivative of ε_1 at the boundary of the instability region.

FLD concept is very useful tool in sheet metal forming finite element analysis (FEA). Numerical evaluation of the forming operations formability is usually performed by confronting strains estimated in numerical simulation with the FLC. This analysis allows us to determine that the strains assumed for the formed material are above the FLC but we are not able to determine a failure point in the simulation itself.

The present work aims to compare the two criteria of strain localization applied in the numerical and experimental analysis of the Nakajima formability test. Investigations have been carried out for DC04 grade steel sheet. Two specimens with different strain paths for these comparisons have been chosen. The onset of localized necking has been determined using the criteria studied in the authors' earlier works, based on the analysis of the principal strains evolution in time. The first criterion is based on the analysis of the through-thickness thinning (through-thickness strain) and its first time derivative in the most strained zone. The maximum of the strain acceleration determines the limit strain in the second method. Limit strains obtained from these criteria have been confronted with the experimental FLC evaluated according to the ISO 12004-2 standard.

The outline of this paper is as follows. The experimental results of the Nakajima test are briefly described in the section 2, then the two algorithms for determination of limit strains, which are used in this work, are described in section 3. These algorithms are applied to experimental and numerical results shown in section 4. Finally, conclusions drawn from this work are given.

2. Experimental results

Nakajima formability tests have been carried out for the steel sheet grade DC04 0.85 mm thick. The tests have been performed using a PTFE foil between the sheet and punch. Six samples with width ranging from 30 to 180 mm have been used to build the FLC. Results from tests for selected two specimens presented in figure 1 have been used for validation of numerical results. These specimens (30mm width and circular with 180 mm diameter) related to the uniaxial and biaxial strain paths. The GOM ARAMIS system has been used to measure strains on the surface of the sample and to analyze the deformation. The experimental FLC shown in figure 2 has been built using the GOM ARAMIS software according to ISO 12004-2 [4].

3. Methods for determination of limit strains

The criteria to determine the strain localization have been applied to the most strained locations in the samples identified from the strain distributions in the experiment or numerical analysis. The evolution of the principal strains and thinning rate have been presented in Fig. 3a. Two criteria have been applied to analyze the strain evolution.

The limit strain in the first criterion proposed by Volk and Hora [8] is defined by the point corresponding to a sudden change of the slope of the thinning rate vs. time curve. The critical

Figure 1. Sample fractured specimens: (a) 30 mm wide, (b) circular (180 mm diameter).

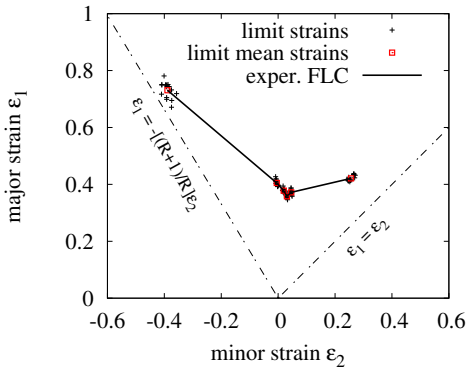

Figure 2. Forming limit diagram with experimental FLC.

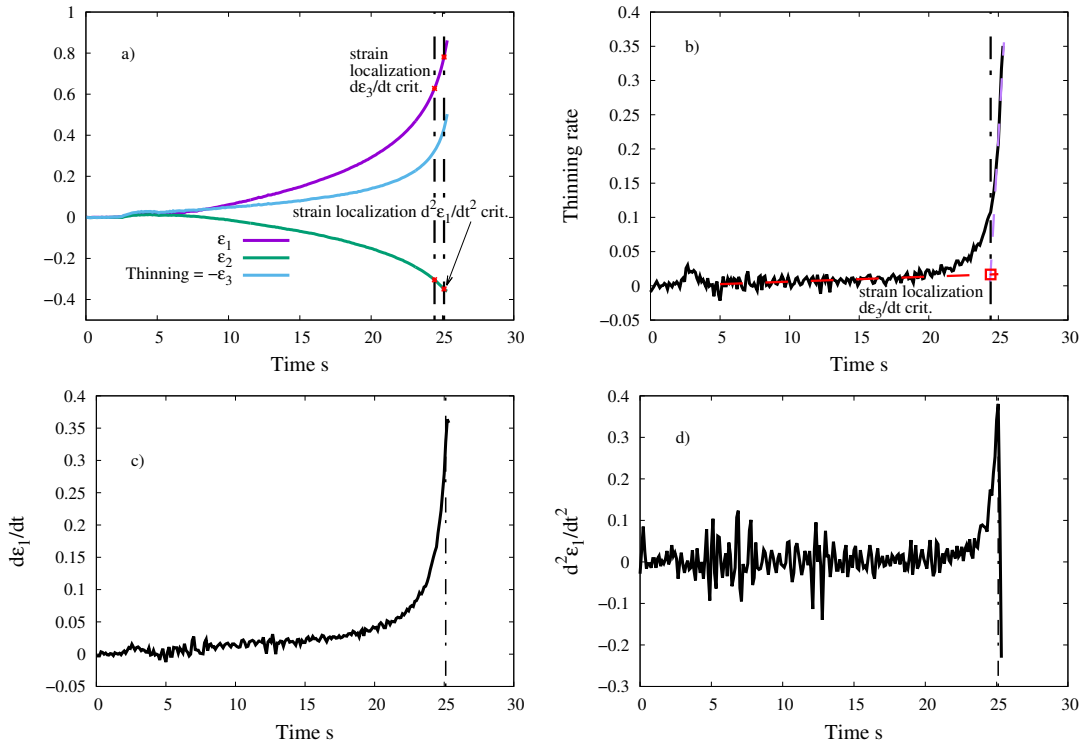

Figure 3. Determination of the onset of localized necking in the experiment for the specimen 30 mm wide: a) evolution of principal strains, b) thinning rate history, c) major principal strain rate history, d) major principal strain acceleration history in the failure zone.

point in Fig. 3b is determined by the intersection of the extensions of approximately straight segments of the thinning rate curve before and after necking. The intersection corresponds to the time $t = 24.4$ s. Thus, the limit principal strains for the considered specimen, are given by the values of the minor and major principal strain at time $t = 24.4$ s, $\varepsilon_1 = 0.639$ and $\varepsilon_2 = -0.313$. According to the second criterion presented by Situ et al. [6], the strain localization is determined by the inflection point in the major strain rate curve shown in Fig.

3c. The inflection point corresponds to the maximum of the major strain acceleration curve plotted in Fig. 3d. The maximum is achieved at the time $t = 25$ s, and the point of strain localization for the considered specimen, is given by the values of the minor and major principal strains at this time, $\varepsilon_1 = 0.772$ and $\varepsilon_2 = -0.35$. Both criteria will be used in the same manner to analyze strains in the most strained locations in the other studied specimens identified from the strain distributions determined experimentally and numerically.

4. Numerical model and simulation results

The Nakajima test has been simulated in authors own computer explicit dynamic finite element program [10, 11]. Sheet metal specimen has been discretized by BST (Basic Shell Triangle) elements [12]. The material has been considered using the Hill48 constitutive model with planar anisotropy which is generally agreed that is sufficiently accurate for the DC04 steel.

Material properties of the DC04 sheet have been determined from tensile tests of the specimens cut at the different orientation with respect to the rolling direction. The stress-strain curve fitting the average results of tensile tests has been taken in the following form:

$$\sigma_{\mathrm{y}}\left(\bar{\varepsilon}_{\mathrm{p}}\right) = K(\varepsilon_0 + \bar{\varepsilon}_{\mathrm{p}})^n = 528(0.0097 + \bar{\varepsilon}_{\mathrm{p}})^{0.205} \text{ MPa} \tag{1}$$

Anisotropy has been defined by the Lankford coefficients $r_0 = 1.96$, $r_{45} = 1.3$, $r_{90} = 2.19$. The simulations have been carried out using a simplified geometrical model, taking into account higher friction between the blank holder, die, and sheet instead of modeling the drawbead. This has allowed us to reduce the number of elements considerably and to avoid very small elements limiting the time step length.

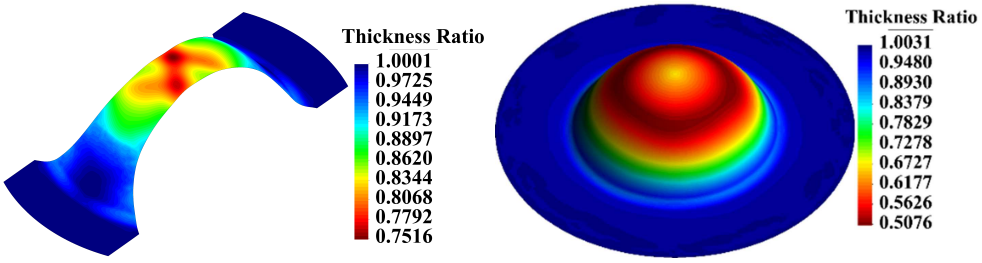

Figure 4. Thickness ratio (deformed to initial thickness) distribution at the end of simulation on deformed shapes of the specimens: a) 30 mm wide, b) circular with the diameter of 180 mm.

Simulations have been performed for two specimens: with width of 30 and one full circular specimen with the diameter of 180 mm. Figure 4 shows deformed shapes of the two samples with the thickness ratio (deformed to initial thickness) distribution at the end of the simulation. The level of stamping at which the failure in the form of necking is achieved in numerical simulation has been assessed using the same presented procedure as applied to determine limit strains in the experiment. Results of the determination of the onset of localized necking in numerical simulation and experiment have been shown for the 30 mm wide and circular specimens in Tab.1.

The forming limit diagram with strains corresponding to these samples is given in Fig. 5a and the strain paths for the most strained locations of these specimens until the critical state have been plotted in the FLD shown in Fig. 5b. To obtain strain paths for these specimens as close as possible to the experimental strain paths (Fig. 5) calibration procedure for the friction, conditions have been performed. Friction conditions between the punch and sheet have been analyzed for several friction values, and by the inverse analysis, it was found that for the

Table 1. Determined limit principal (ε_1 major and ε_2 minor) strains in numerical simulation and experiment.

analysis type	thinning rate evolution criterion			maximum strain acceleration criterion		
	time s	major strain ε_1	minor strain,ε_2	time	major strain ε_1	minor strain ε_2
numerical 30 mm	3.81e-3	0.697	-0.394	4.03e-3	0.46	-0.019
experimental 30 mm	24.4	0.639	-0.313	25.0	0.772	-0.35
numerical circular	4.1e-3	0.42	0.227	4.19e-3	0.493	0.237
experimental circular	37.3	0.4317	0.253	38	0.489	0.2614

specimen 30 mm wide friction coefficient assessed value $\mu = 0.05$ and the full circular specimen with $\mu = 0.1$. The differences in process time between experiment ($v = 75$ mm/min) and simulation ($v = 10$ m/s) result from the fact that the punch speed in the simulation was higher than the speed in the experiment. By increasing the punch speed [13], the total simulation time has been reduced.

It can be seen both in Table 1 and in Fig. 5 that the thinning rate evolution criterion gives the values of limit strains are close to the experimental ones. The maximum strain acceleration criterion, in turn, overestimates the limit strains while compared to the experimental FLC according to the ISO norm. Furthermore, experimental and numerical strains are close to the values of strains before the fracture.

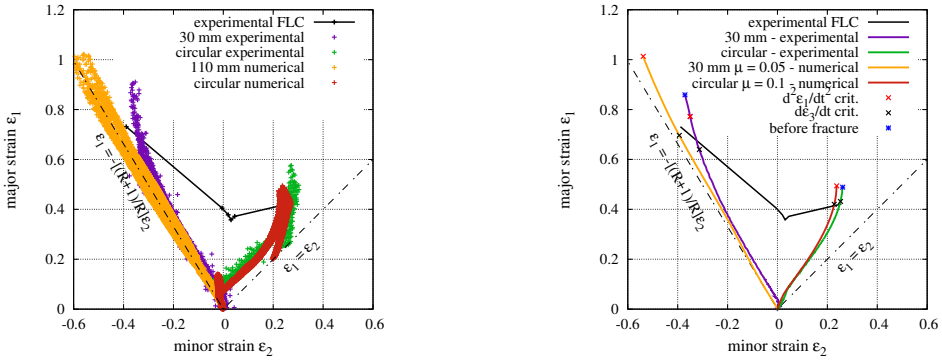

a) b)

Figure 5. Comparison between simulated and experimentally measured principal in-plane strains plotted on the a) FLD and b) limit strains for experimental and numerical strain paths compared with the experimental FLC.

The comparison between experimental and numerically predicted drawing force in the function of punch displacement is presented in Fig. 6. Points corresponding to moments of localization determined by the different criteria have been shown in Fig. 6. Maximum strain acceleration criterion predicts limit strains which correspond to the higher force and punch displacement value closer to the maxim force.

It can be seen that Hill48 model with the material parameters from tensile tests, overestimates the force-displacement response which is also observed by other authors [3]. Nevertheless, the limit strains determined from numerical simulations and in experiments are close to each other.

5. Conclusions

Investigation of numerical results received in simulations of Nakajima tests done for the selected specimens proves the validity of the developed numerical model. Limit strains obtained

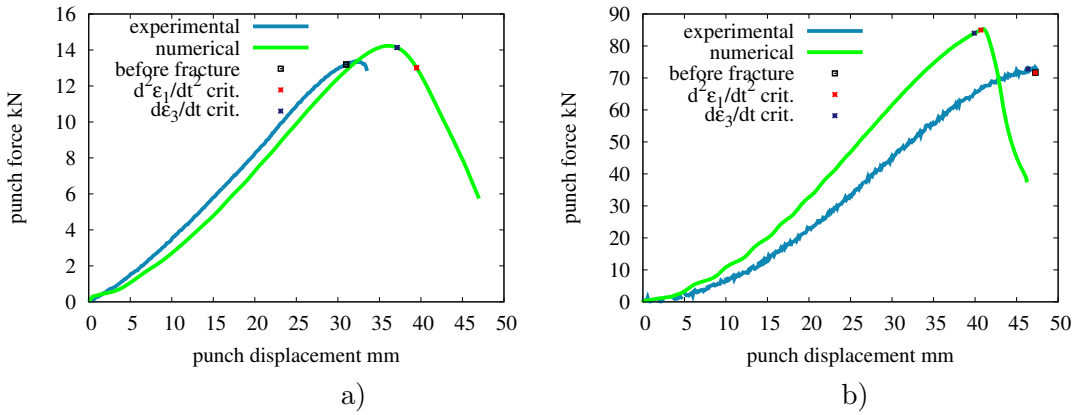

Figure 6. The comparison between numerical and experimental drawing force response in Nakajima formability test for the specimen: a) 30 mm wide, b) circular with the diameter of 180 mm.

experimentally and numerically have been compared to experimental FLC. A closer prediction with the FLC has been achieved from the first criterion based on the change of the slope of the thinning rate.

The second criterion which is based on the maximum strain acceleration gives values of strains higher than FLC determined according to ISO 12004-2 norm. These values are closer to the strains corresponding to fracture limit. Both criteria predict failure at the time step close to the maximum punch force. The results show that investigated time-dependent methods allow determining strain localization in numerical simulation and experimental studies.

References

[1] Sheng Z and Mallick P 2017 *International Journal of Mechanical Sciences* **128-129** 345 – 360
[2] Hu Q, Zhang L, Ouyang Q, Li X, Zhu X and Chen J 2018 *International Journal of Plasticity* **103** 143 – 167
[3] Lian J, Shen F, Jia X, Ahn D C, Chae D C, Mnstermann S and Bleck W 2017 *International Journal of Solids and Structures*
[4] ISO 12004-2 2008 *Metallic materials – Sheet and strip – Determination of forming-limit curves. Part 2: Determination of forming-limit curves in the laboratory*
[5] Marciniak Z 1994 *Archiwum Mechaniki Stosorwanej* **17** 577–592
[6] Situ Q, Jain M and Metzger D 2011 *Int. Journal of Mechanical Sciences* **53** 707–719
[7] Banabic D 2010 *Sheet Metal Forming Processes Constitutive Modelling and Numerical Simulation* (Springer)
[8] Volk W and Hora P 2011 *International Journal of Material Forming* **4** 339–346
[9] Martnez-Donaire A, Garca-Lomas F and Vallellano C 2014 *Materials Design* **57** 135 – 145
[10] Lumelskyj D, Rojek J, Banabic D and Lazarescu L 2017 *Procedia Engineering* **183** 89 – 94 17th International Conference on Sheet Metal, SHEMET17
[11] Lumelskyy D, Rojek J, R P, Grosman F and Tkocz M 2012 *Archives of Civil and Mechanical Engineering* **12** 133–141
[12] Rojek J and Oñate E 1998 *International Journal of Forming Processes* **1** 275–296
[13] Jung D W 1998 *Journal of Materials Engineering and Performance* **7** 479–490